Geophysical Journal International

Geophys. J. Int. (2013) **194,** 118–124
Advance Access publication 2013 April 18

doi: 10.1093/gji/ggt116

The deep seismic structure of the Ethiopia/Afar hotspot and the African superplume

Samantha E. Hansen[1] and Andrew A. Nyblade[2]

[1]*Geological Sciences Department, The University of Alabama, Tuscaloosa, Alabama,* 35487*, USA. E-mail: shansen@geo.ua.edu*
[2]*Geosciences Department, The Pennsylvania State University, University Park, Pennsylvania,* 16802*, USA*

Accepted 2013 March 20. Received 2013 March 19; in original form 2012 October 21

SUMMARY

The Ethiopia/Afar hotspot has been frequently explained as an upper mantle continuation of the African superplume, with anomalous material in the lower mantle under southern Africa, rising through the transition zone beneath eastern Africa. However, the significantly larger amplitude low velocity anomaly in the upper mantle beneath Ethiopia/Afar, compared to the anomalies beneath neighboring regions, has led to questions about whether or not along-strike differences in the seismic structure beneath eastern Africa and western Arabia are consistent with the superplume interpretation. Here we present a new *P*-wave model of the hotspot's deep structure and use it to evaluate the superplume model. At shallow ($< \sim$400 km) depths, the slowest velocities are centered beneath the Main Ethiopian Rift, and we attribute these low velocities to decompression melting beneath young, thin lithosphere. At deeper depths, the low velocity structure trends to the northeast, and the locus of the low velocity anomaly is found beneath Afar. The northeast-trending structure with depth is best modeled by northeastward flow of warm superplume material beneath eastern Africa. The combined effects of shallow decompression melting and northeastward flow of superplume material explain why upper mantle velocities beneath Ethiopia/Afar are significantly slower than those beneath neighboring East Africa and western Arabia. The superplume interpretation can thus explain the deep seismic structure of the hotspot if the effects of both decompression melting and mantle flow are considered.

Key words: Ethiopia; Afar; hotspot; superplume; tomography.

INTRODUCTION

The Ethiopia/Afar hotspot is one of the most prominent geophysical and geochemical anomalies on Earth and its origin, like that of many other hotspots, is still widely debated. Seismic tomography studies of the upper mantle published over the past decade have called into question models invoking plume heads because the low velocity anomaly in the mantle beneath Ethiopia/Afar is too deep and too wide to be readily explained by a simple plume model (e.g., Bastow *et al.* 2005, 2008; Benoit *et al.* 2006a,b). The hotspot has also been frequently explained as an upper mantle continuation of the African superplume, a broad, anomalous upwelling that originates in the lower mantle beneath southern Africa (e.g. Ritsema *et al.* 1999; Ritsema & Allen 2003; Simmons *et al.* 2007, 2009; Forte *et al.* 2010), and there are a growing number of geochemical studies that also support this interpretation (e.g. Marty *et al.* 1996; Pik *et al.* 2006; Hilton *et al.* 2011).

Hansen *et al.* (2012) recently demonstrated that the superplume structure likely crosses the transition zone from the lower to the upper mantle beneath northern Zambia or southern Tanzania (Fig. S1) and suggested that flow of anomalously warm superplume material may continue within the upper mantle to the northeast under Kenya, Ethiopia, Afar, and western Arabia. However, the significantly larger amplitude low velocity anomaly in the upper mantle beneath Ethiopia/Afar, compared to anomalies beneath neighboring East Africa and western Arabia (Fig. S1), has led to questions about whether or not along-strike differences in the seismic structure beneath eastern Africa and Arabia are consistent with the superplume interpretation.

Differences in the geographic locus of the seismic anomaly between tomographic models have also contributed to questions about the superplume interpretation. For instance, many global studies (e.g. Ritsema & Allen 2003; Montelli *et al.* 2006; Simmons *et al.* 2011) show the slowest velocities beneath the Afar Depression (Fig. 1), which has long been interpreted as the center of the hotspot. However, some higher-resolution regional-scale models (*e.g.,* Bastow *et al.* 2005, 2008; Benoit *et al.* 2006a,b) show that the most pronounced low velocities are beneath the Main Ethiopian Rift (MER) to the southwest of Afar.

Here we present a new image of mantle *P*-wave velocity variations beneath Ethiopia/Afar and use it to evaluate the superplume model. The velocity image has been developed using a global

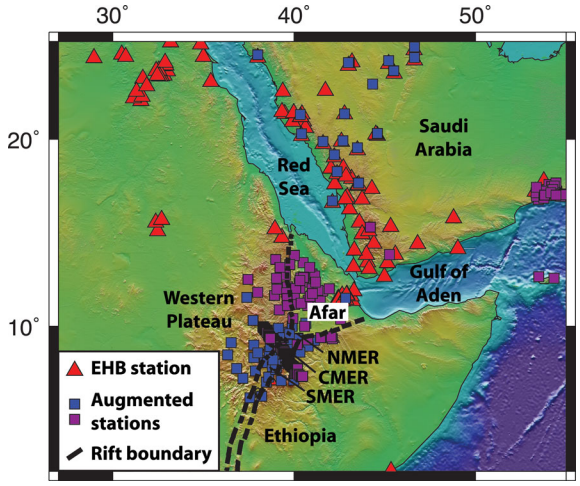

Figure 1. Map of the study region with 30 s digital topography (Wessel & Smith 1998). Red triangles: EHB catalog stations, blue squares: augmented stations also used by Hansen *et al.* (2012), purple squares: new augmented stations. Bold dashed lines: MER boundaries. NMER/CMER/SMER: northern/central/southern Main Ethiopian Rift.

tomographic inversion and a dataset containing travel-times from earthquakes recorded on many new seismic stations within Ethiopia, Afar, and across the study region, thereby providing improved resolution over the Hansen *et al.* (2012) model. Our image reveals important features of the low velocity zone (LVZ) beneath Ethiopia/Afar, which we use to show that the deep seismic structure of the hotspot is consistent with the superplume interpretation.

ADAPTIVELY PARAMETERIZED TOMOGRAPHY

The new *P*-wave image has been developed using an adaptive parameterization approach (Kárason 2002; Li *et al.* 2008), described in detail by Hansen *et al.* (2012). This tomographic approach uses travel-time residuals calculated with respect to travel-times predicted by the ak135 Earth model (Kennett *et al.* 1995). The largest source of travel-time residuals used is the reprocessed International Seismological Centre database (Engdahl *et al.* 1998; hereinafter referred to as the EHB database), which includes over 15 million travel-time residuals from more than 496,000 earthquakes between January 1964 and October 2007 (Fig. S2).

Many of the African stations included in the EHB database only operated for short periods of time and their distribution is sparse compared to many other regions of the globe. Therefore, we have augmented the EHB dataset with *P*-wave travel-times recorded by new permanent AfricaArray (www.africaarray.org) seismic stations as well as by temporary seismic networks operated over the past two decades (Fig. 1; Fig. S2). Compared to Hansen *et al.* (2012), the dataset employed here includes an additional 14 592 travel-time measurements from 187 new stations in and around Ethiopia and Afar, greatly improving coverage of the study region.

The dataset was inverted for a global model of mantle *P*-wave structure. Significant lateral variations in resolution may result from uneven seismic raypath coverage in the mantle, and most tomographic techniques use a regularly-spaced grid, which tends to either over-emphasize poorly sampled regions or average out small-scale structure. To mitigate the effects of uneven data coverage, the tomographic method employed here constructs an adaptable grid based on the sampling density of the data (Kárason 2002). The adaptive grid is developed by combining one or more cells from a base grid until a minimum ray density in each cell is achieved (Kárason 2002; Li *et al.* 2008; Hansen *et al.* 2012), resulting in a finer grid spacing for regions with increased ray coverage (Fig. S3). The small incidence angles of *P*-waves may cause crustal anomalies to 'smear' to deeper depths in the model; therefore the inversion also takes crustal structure into account using an *a priori* 3-D crustal model (CRUST2.0; Bassin *et al.* 2000). This approach balances the crust and upper mantle contributions to the misfit (Li *et al.* 2006, 2008).

Kárason (2002) and Li *et al.* (2008) provide a full description of the sensitivity matrix calculations. Briefly, for short-period data with a center frequency of ∼1 Hz, the data are back-projected along raypaths calculated in the ak135 reference model. Weighted composite rays are used to reduce the size of the sensitivity matrix (Spakman & Nolet 1988; Kárason & van der Hilst 2001). For long-period data, 3-D sensitivity kernels are approximated following Kárason & van der Hilst (2001). This approach allows the low-frequency data to constrain long wavelength structure without preventing short-period data from resolving smaller scale structures.

Although our inversion solves for the full mantle structure (Fig. S1), we are primarily interested in the upper mantle variations beneath Ethiopia and Afar. Fig. 2a shows the *P*-wave velocity perturbations relative to the ak135 reference model (δV_p) at selected upper mantle depths beneath the study region. These results were obtained after 200 iterations of the inversion and correspond to a 92 per cent reduction of the error function. The length of the residual vector dropped from 0.95 to 0.31 s. While all of eastern Africa is underlain by slow velocities, at depths $<$ ∼400 km the slowest velocities ($\delta V_p \sim -3$ per cent) are concentrated beneath the central and northern MER, with the center of the LVZ situated slightly to the northwest of the rift axis. At deeper depths ($>$ ∼400 km), the center of the LVZ shifts to the northeast beneath Afar. This can also be seen in cross-section (Fig. 2b), where the low velocities have a northeast trend with depth. Checkerboard resolution tests illustrate that the amplitude recovery in the model is ∼30–50 per cent (Fig. S4). This is due, in a large part, to regularization parameters used in the inversion to suppress the effects of noise in the data.

DISCUSSION

At shallow mantle depths ($<$ ∼400 km), our tomographic results show the locus of the hotspot anomaly beneath the MER, similar to a number of regional studies (Bastow *et al.* 2005, 2008; Benoit *et al.* 2006a,b). However, at deeper depths, our image of δV_p is more similar to other global and regional tomography models (e.g. Ritsema & Allen 2003; Montelli *et al.* 2006; Chang & Van der Lee 2011; Simmons *et al.* 2011, 2012), which show the anomaly centered beneath Afar. Bastow *et al.* (2008) suggested that the shallow LVZ structure beneath the MER could result from either enhanced decompression melting beneath young, thin lithosphere and/or from focused mantle flow. Other studies have also explored these options. For instance, Rychert *et al.* (2012) argued that the geodynamics in this region can be explained by decompression melting with little or no influence from mantle upwelling. Hammond *et al.* (2013) also advocated for near-surface melting but suggested that density-driven flow deeper in the mantle also contributes to the seismic structure.

Using a synthetic anomaly in the upper mantle, we have simulated the LVZ beneath the MER to assess whether the observed low velocities can be attributed purely to decompression melting beneath thin lithosphere (Fig. 3a). The depth extent of decompression melting beneath Ethiopia is not well constrained, but petrologic studies

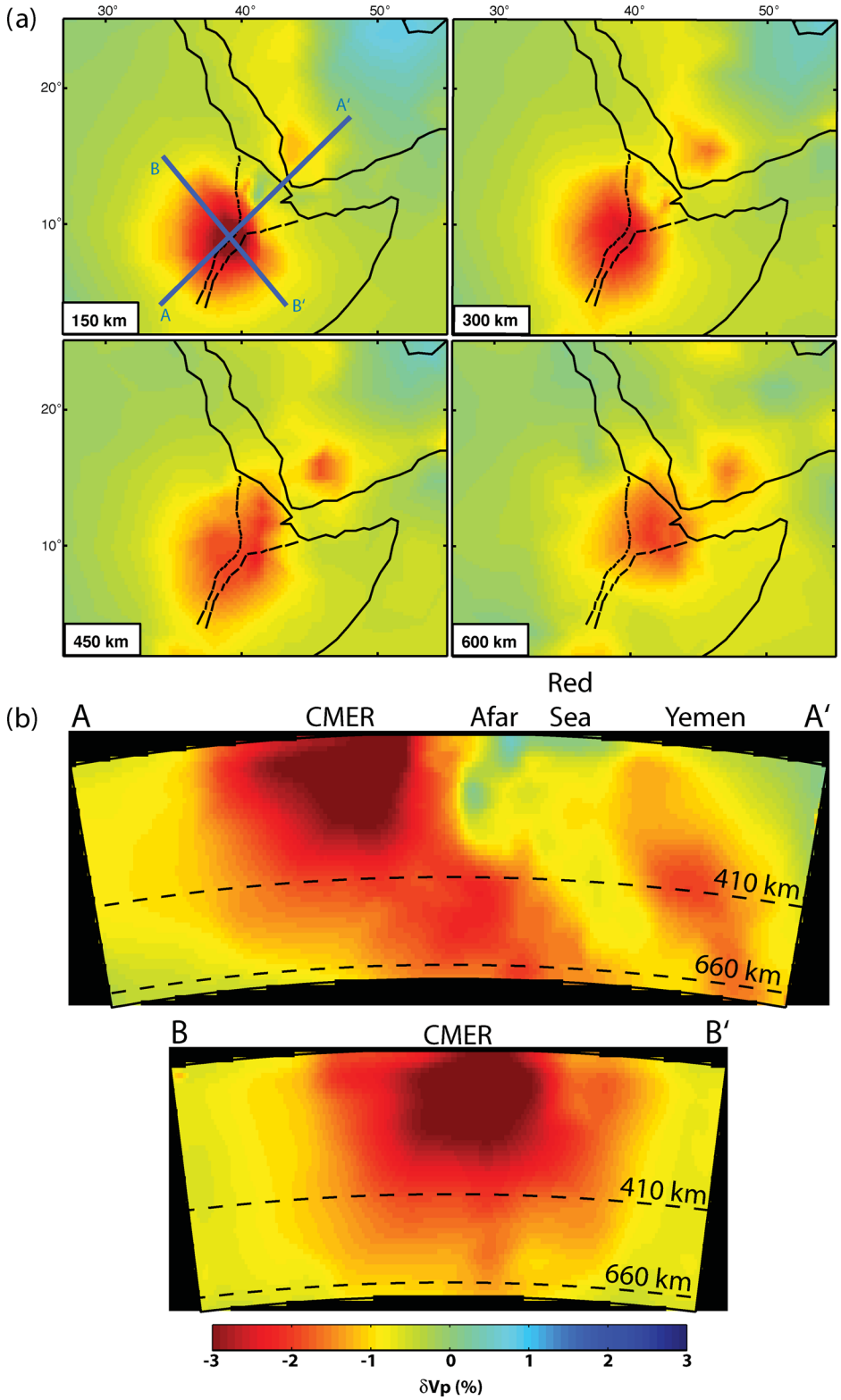

Figure 2. (a) *P*-wave velocity perturbations relative to the ak135 reference model (δV_p) at selected upper mantle depths. Bold dashed lines: MER boundaries. Two profiles, A-A′ and B-B′, are shown in the 150 km depth panel. Profile A-A′ passes through the center of the LVZ. Profile B-B′ is perpendicular to profile A-A′ and runs through the center of the slowest part of the LVZ. (b) Cross-sections along both profiles A-A′ and B-B′. Dashed lines: 410 and 660 km discontinuities. All panels have been plotted with a ± 3 per cent color scale.

estimate the melting depth beneath Afar is ∼70–90 km (Furman 2007, and references therein). Therefore, we use an 80-km thick synthetic anomaly in our model (Fig. 3a). Given our amplitude recovery at these depths, the corresponding input amplitude has been set to −6 per cent, which is comparable to that estimated by Bastow *et al.* (2008). Synthetic travel-times were created and inverted using the same model parameterization as was used for the data. Noise was added to the synthetic travel-times as a Gaussian

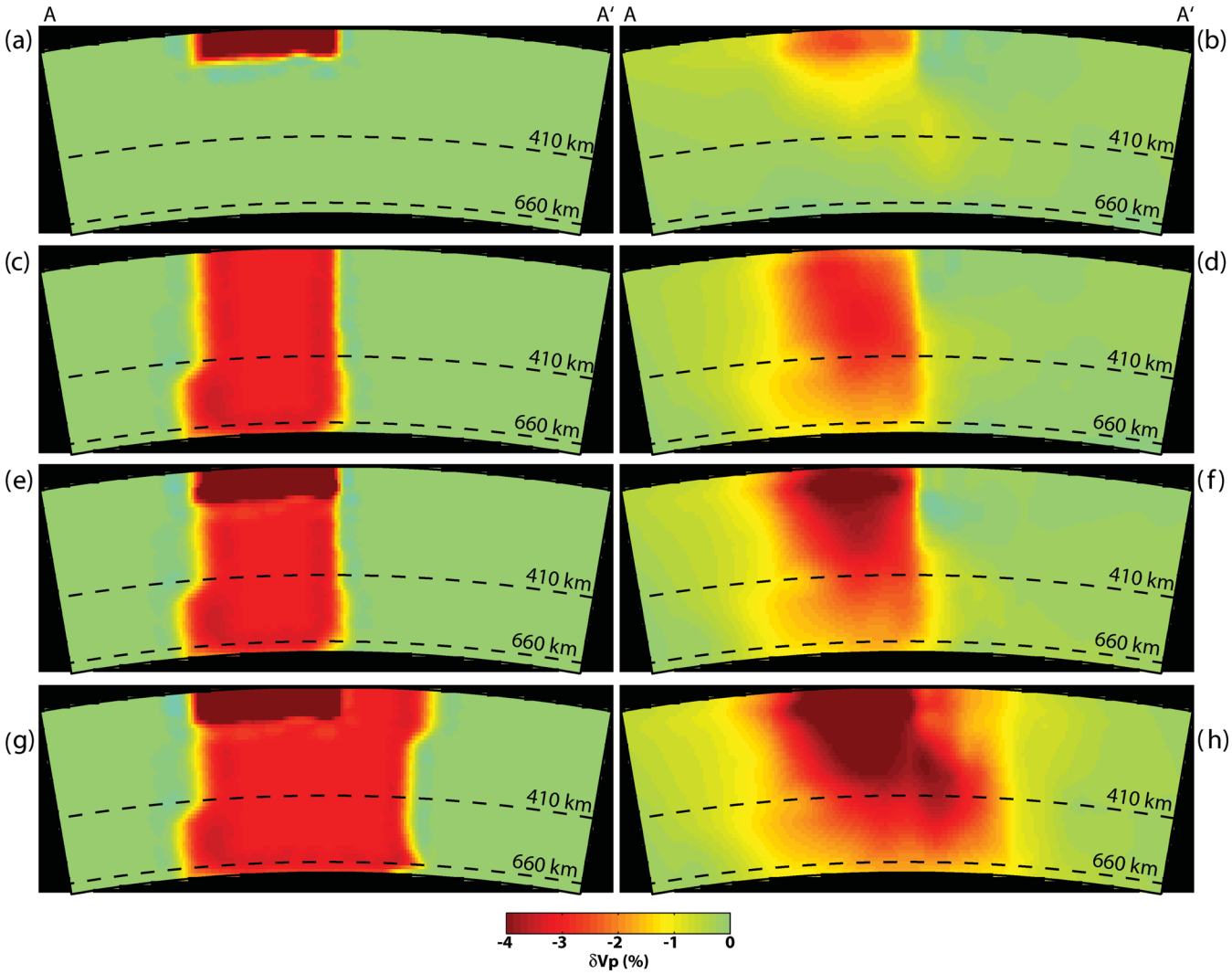

Figure 3. Resolution tests with synthetic anomalies. Left: Input models, Right: recovered models. All anomalies have been projected onto the adaptive grid (Fig. S3). δV_p indicates velocity perturbations relative to the ak135 reference model. (a–b) 80-km thick anomaly situated beneath the MER to simulate decompression melting in the upper mantle. The input amplitude was set to a constant −6 per cent, as described in the text. (c–d) Anomaly representing focused mantle flow beneath the MER with no decompression melting. The corresponding input amplitude is −3 per cent. (e–f) A combined model with both decompression melting and focused mantle upwelling represented by the anomalies. Input amplitudes are the same as those used in panels (a) and (c). (g–h) Same as (e–f) but now the 'mantle flow' anomaly extends laterally beneath Afar.

residual time error with a standard deviation of 0.3 s, which is the residual remaining in our model after inversion. The recovered image (Fig. 3b) shows ∼150 km of vertical smearing, which is not atypical for *P*-wave tomography studies (e.g. Benoit *et al.* 2003, 2006b; Park *et al.* 2007); however, the results do not match the observed low velocities beneath Ethiopia/Afar, which extend down through the transition zone (Fig. 2b). In addition, we have also examined a ∼200 km thick synthetic anomaly, which is the maximum depth estimated for decompression melting beneath rapidly thinning lithosphere (e.g. Webb & Forsyth 1998), but these results also failed to match our observations (Figs S5a–b). Therefore, decompression melting cannot be the only factor contributing to the observed seismic anomaly.

We have also investigated the possibility of focused mantle flow beneath the MER (Fig. 3c). In this case, the synthetic input anomaly has an amplitude of −3 per cent and extends from the surface to the base of the transition zone, similar to synthetic tests performed by Hansen *et al.* (2012). The results (Fig. 3d) better match the depth extent of the imaged LVZ (Fig. 2), but neither the pronounced low velocities at shallow depths beneath the MER nor the low velocities at depths > ∼400 km beneath Afar are observed.

To investigate the combined effects of decompression melting and mantle flow, additional modeling tests have been performed. As in the previous cases (Figs 3a and c; Fig. S5a), a −6 per cent synthetic anomaly was used to simulate decompression melting beneath the MER, and a −3 per cent anomaly is used to represent mantle flow (Fig. 3e; Fig. S5c). The recovered image (Fig. 3f; Fig. S5d) provides a reasonable match to the pronounced low velocities observed beneath the MER in our tomographic model as well as the continuation of the low velocities through the transition zone (Fig. 2). However, a key difference between our observed anomaly (Fig. 2) and the recovered synthetic image (Fig. 3f) is the northeast trend of the low velocities with depth. This trend can be better simulated by allowing the synthetic 'mantle flow' anomaly to extend laterally to the northeast beneath both the MER and Afar (Figs 3g–h; Figs S5e–f).

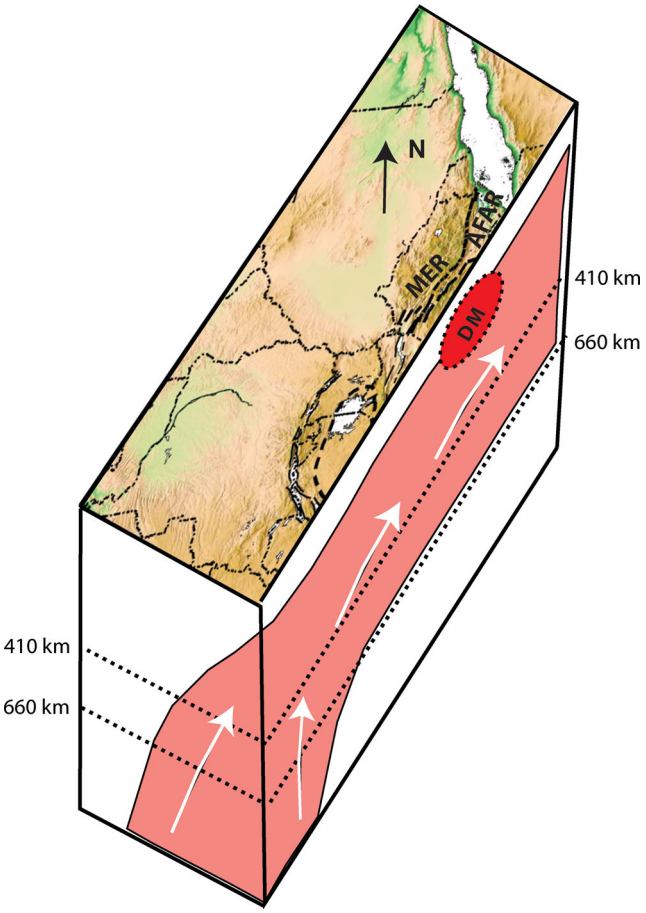

Figure 4. Cartoon illustrating our interpretation of the mantle structure beneath eastern Africa. Pink shaded region and white arrows indicate the flow of superplume material. DM: decompression melting; MER: Main Ethiopian Rift.

To summarize, the depth-dependent structure of the LVZ in our model can be explained by a combination of decompression melting at shallow mantle depths beneath the MER and warm material throughout the upper mantle beneath both the MER and Afar, but not by either phenomena alone. The combined effects are needed to explain the depth extent of the LVZ, the northeast trend of the LVZ with depth, and why the amplitude of the velocity anomaly beneath Ethiopia/Afar is significantly greater than those beneath neighboring East Africa and western Arabia. Some decompression melting beneath Afar cannot be ruled out (e.g. Hammond *et al.* 2013), but our model and resolution tests suggest more extensive melting beneath the MER.

The finding that decompression melting beneath the MER is contributing significantly to the LVZ structure is in accord with geological evidence showing young, thin lithosphere beneath the central and northern parts of the MER (Ebinger & Casey 2001; Bonini *et al.* 2005; Rooney *et al.* 2007; Bastow *et al.* 2008; Keranen & Klemperer 2008; Abebe *et al.* 2010). The warm material throughout the upper mantle beneath the MER and Afar can be readily attributed to northeast-directed flow of anomalous African superplume material (Fig. 4). As noted in the introduction, Hansen *et al.* (2012) suggested that warm superplume material crosses the transition zone from the lower to the upper mantle beneath northern Zambia or southern Tanzania and that the flow of this material may continue within the upper mantle to the northeast under Kenya, Ethiopia, Afar, and western Arabia. The full mantle structure obtained in the current study shows a similar pattern to that shown by Hansen *et al.* (2012), consistent with these interpretations (Fig. S1). Additionally, the northeastward trend of the LVZ with depth beneath Afar highlighted by our current model (Fig. 2) is consistent with superplume material flowing from southwest to northeast beneath East Africa, Ethiopia, and Afar (Fig. 4). Patterns of seismic anisotropy revealed by shear-wave splitting measurements also suggest a northeastward flow field in the upper mantle beneath this region (Gao *et al.* 2010; Bagley & Nyblade 2013).

The northeasterly-directed flow field, as illustrated in Fig. 4, is idealized in that it does not reflect perturbations that may arise from variations in lithospheric structure. Such variations could direct anomalous mantle material around regions of thicker lithosphere, such as that found beneath the Tanzania craton (Bagley & Nyblade 2013), or focus it to shallower depths beneath regions of thinner lithosphere. Nevertheless, while complexities in the flow field associated with the African superplume are likely to exist, a dominant northeasterly-directed flow is sufficient to explain the origin of the warm material throughout the upper mantle beneath the MER and Afar.

The northeasterly trend of the LVZ with depth (Fig. 2) can also help to explain differences between tomographic images of the hotspot anomaly. Regional models which show the center of the hotspot anomaly beneath the MER may better resolve the shallow LVZ caused by decompression melting, while global models may better resolve the deeper mantle structure beneath Afar. The adaptive parameterization approach, coupled with the expanded travel-time dataset, employed here allows us to help bridge this resolution gap.

CONCLUSIONS

We have developed a new *P*-wave velocity model to evaluate the superplume interpretation for the Ethiopia/Afar hotspot. At shallow ($< \sim$400 km) depths, the slowest velocities are centered beneath the central and northern MER, and we attribute these low velocities mainly to decompression melting beneath young, thin lithosphere. At deeper depths, the low velocity structure trends to the northeast, and the locus of the LVZ is found beneath Afar. The northeast trend of the LVZ is best modeled by northward flow of warm superplume material beneath eastern Africa, and the combined effects of decompression melting and northward flow of superplume material explain why the LVZ beneath the Ethiopia/Afar hotspot is more pronounced than low velocities beneath East Africa and western Arabia. The superplume model for the hotspot is thus consistent with the deep seismic structure of the mantle beneath Ethiopia and Afar if the effects of both decompression melting and mantle flow are considered.

ACKNOWLEDGEMENTS

We thank A. Reusch, I. Bastow, M. Benoit, G. Mulibo, and Y. Park for providing the *P*-wave travel-time data from their respective studies, R. van der Hilst and S. Burdick for providing the tomography software, and two anonymous reviewers for their thorough critiques of this manuscript. The Incorporated Research Institutions for Seismology (IRIS) Data Management System provided data handling assistance, and funding for this project was provided by the National Science Foundation (grant numbers OISE 0530062, EAR 0824781, and EAR 0440032).

REFERENCES

Abebe, T., Balestrieri, M. & Bigazzi, G., 2010. The Central Main Ethiopian Rift is younger than 8 Ma: confirmation through apatite fission-track thermochronology, *Terra Nova,* **22,** 470–476.

Bagley, B. & Nyblade, A., 2013. Seismic anisotropy in eastern Africa, mantle flow, and the African superplume, *Geophys. Res. Lett.,* in press, doi:10.1002/grl.50315.

Bassin, C., Laske, G. & Masters, G., 2000. The current limits of resolution for surface wave tomography in North America, *Eos Trans. AGU,* **81**(48), Fall Meet. Suppl., Abstract S12A-03.

Bastow, I., Stuart, G., Kendall, J.-M. & Ebinger, C., 2005. Upper-mantle seismic structure in a region of incipient continental breakup: northern Ethiopian rift, *Geophys. J. Int.,* **162,** 479–493.

Bastow, I., Nyblade, A., Stuart, G., Rooney, T. & Benoit, M., 2008. Upper mantle seismic structure beneath the Ethiopian hot spot: Rifting at the edge of the African low-velocity anomaly, *Geochem. Geophys. Geosyst.,* **9,** doi:10.1029/2008GC002107.

Benoit, M., Nyblade, A., VanDecar, J. & Gurrola, H., 2003. Upper mantle *P*-wave velocity structure and transition zone thickness beneath the Arabian Shield, *Geophys. Res. Lett.,* **30,** doi:10.1029/2002GL016436.

Benoit, M., Nyblade, A., Owens, T. & Stuart, G., 2006a. Mantle transition zone structure and upper mantle S velocity variations beneath Ethiopia: Evidence for a broad, deep-seated thermal anomaly, *Geochem. Geophys. Geosyst.,* **7,** doi:10.1029/2006GC001398.

Benoit, M., Nyblade, A. & VanDecar, J., 2006b. Upper mantle *P*-wave speed variations beneath Ethiopia and the origin of the Afar hotspot, *Geology,* **34,** 329–332.

Bonini, M., Corti, G., Innocenti, F., Manetti, P., Mazzarini, F., Abebe, T. & Pecskay, Z., 2005. Evolution of the Main Ethiopian Rift in the fram of Afar and Kenya rifts propagation, *Tectonics,* **24,** doi:10.1029/2004TC001680.

Chang, S.-J. & Van der Lee, S., 2011. Mantle plumes and associated flow beneath Arabia and East Africa, *Earth Planet. Sci. Lett.,* doi:10.1016/j.epsl.2010.12.050.

Ebinger, C. & Casey, M., 2001. Continental breakup in magmatic provinces: an Ethiopian example, *Geology,* **29,** 527–530.

Engdahl, E., van der Hilst, R. & Buland, R., 1998. Global teleseismic earthquake relocation with improved travel times and procedures for depth determination, *Bull. seism. Soc. Am.,* **88,** 722–743.

Forte, A., Quéré, S., Moucha, R., Simmons, N., Grand, S., Mitrovica, J. & Rowley, D., 2010. Joint seismic-geodynamic-mineral physical modeling of African geodynamics: a reconciliation of deep-mantle convection with surface geophysical constraints, *Earth Planet. Sci. Lett.,* **295,** 329–341.

Furman, T., 2007. Geochemistry of East African Rift basalts: an overview, *J. Afr. Earth Sci.,* **48,** 147–160.

Gao, S., Liu, K. & Abdelsalam, M., 2010. Seismic anisotropy beneath the Afar Depression and adjacent areas: implications for mantle flow, *J. Geophys. Res.,* **115,** doi:10.1029/2009JB007141.

Hammond, J.O.S. *et al.*, 2013. Mantle upwelling and initiation of rift segmentation beneath the Afar Depression, *Geology,* in press, doi:10.1130/G33925.1.

Hansen, S., Nyblade, A. & Benoit, M., 2012. Mantle structure beneath Africa and Arabia from adaptively parameterized *P*-wave tomography: Implications for the origin of Cenozoic Afro-Arabian tectonism, *Earth Planet. Sci. Lett.,* **319–320,** 23–34.

Hilton, D.R., Halldórsson, S.A., Barry, P.H., Fischer, T.P., de Moor, J.M., Ramirez, C.J., Mangasini, F. & Scarsi, P., 2011. Helium isotopes at Rungwe Volcanic Province, Tanzania, and the origin of East African Plateaux, *Geo. Res. Lett.,* **38,** L21304, doi:10.1029/2011GL049589.

Kárason, H. & van der Hilst, R.D., 2001. Tomographic imaging of the lowermost mantle with differential times of refracted and diffracted core phases (PKP, Pdiff), *J. Geophys. Res.,* **106,** 6569–6587.

Kárason, H., 2002. Constraints on Mantle Convection from Seismic Tomography and Flow Modeling, *PhD thesis,* Massachusetts Institute of Technology, Cambridge, MA.

Kennett, B., Engdahl, E. & Buland, R., 1995. Constraints on seismic velocities in the Earth from travel times, *Geophys. J. Int.,* **122,** 108–124.

Keranen, K. & Klemperer, S., 2008. Discontinuous and diachronous evolution of the Main Ethiopian Rift: Implications for development of continental rifts, *Earth Planet. Sci. Lett.,* **265,** 96–111.

Li, C., van der Hilst, R.D. & Toksöz, M.N., 2006. Constraining *P* wave velocity variations in the upper mantle beneath Southeast Asia, *Phys. Earth Planet. Inter.,* **154,** 180–195.

Li, C., van der Hilst, R., Engdahl, E. & Burdick, S., 2008. A new global model for 3-D variations of *P*-wave velocity in the Earth's mantle, *Geochem. Geophys. Geosyst.,* **9,** doi:10.1029/2007GC001806.

Marty, B., Pik, R. & Gezahegn, Y., 1996. Helium isotope variations in Ethiopian plume lavas: Nature of magmatic sources and limit on lower mantle contribution, *Earth Planet. Sci. Lett.,* **144,** 223–237.

Montelli, R., Nolet, G., Dahlen, F. & Masters, G., 2006. A catalogue of deep mantle plumes: New results from finite-frequency tomography, *Geochem. Geophys. Geosyst.,* **7,** doi:10.1029/2006GC001248.

Park, Y., Nyblade, A., Rodgers, A. & Al-Amri, A., 2007. Upper mantle structure beneath the Arabian Peninsula and northern Red Sea from teleseismic body wave tomography: Implications for the origin of Cenozoic uplift and volcanism in the Arabian Shield, *Geochem. Geophys. Geosyst.,* **8,** doi:10.1029/2006GC001566.

Pik, R., Marty, B. & Hilton, D.R., 2006. How many plumes in Africa? The geochemical point of view, *Chem. Geol.,* **226,** 100–114.

Ritsema, J., van Heijst, H. & Woodhouse, J., 1999. Complex shear wave velocity structure beneath Africa and Iceland, *Science,* **286,** 1925–1928.

Ritsema, J. & Allen, R., 2003. The elusive mantle plume, *Earth Planet. Sci. Lett.,* **207,** 1–12.

Rooney, T., Furman, T., Bastow, I., Ayalew, D. & Yirgu, G., 2007. Lithospheric modification during crustal extension in the Main Ethiopian Rift, *J. Geophys. Res.,* **112,** doi:10.1029/2006jb004916.

Rychert, C. *et al.*, 2012. Volcanism in the Afar Rift sustained by decompression melting with minimal plume influence, *Nature Geosc.,* doi:10.1038/NGEO1455.

Simmons, N., Forte, A. & Grand, S., 2007. Thermochemical structure and dynamics of the African superplume, *Geophys. Res. Lett.,* **34,** doi:10.1029/2006GL028009.

Simmons, N., Forte, A. & Grand, S., 2009. Joint seismic, geodynamic and mineral physical constraints on three-dimensional mantle heterogeneity: Implications for the relative importance of thermal versus compositional heterogeneity, *Geophys. J. Int.,* **177,** 1284–1304.

Simmons, N., Myers, S. & Johannesson, G., 2011. Global-scale P wave tomography optimized for prediction of teleseismic and regional travel times for Middle East events: 2. Tomographic inversion, *J. Geophys. Res.,* **116,** doi:10.1029/2010JB007969.

Simmons, N.A., Myers, S.C., Johannesson, G. & Matzel, E., 2012. LLNL-G3Dv3: Global P wave tomography model for improved regional and teleseismic travel time prediction, *J. Geophys. Res.,* **117,** B10302, doi:10.1029/2012JB009525.

Spakman, W. & Nolet, G., 1988. Imaging algorithms, accuracy and resolution in delay time tomography, in *Mathematical Geophysics: A Survey of Recent Developments in Seismology and Geodynamics,* pp. 155–188, ed. Vlaar, N.J.

Webb, S. & Forsyth, D., 1998. Structure of the Upper Mantle Under the EPR from Waveform Inversion of Regional Events, *Science,* **280,** 1227–1229.

Wessel, P. & Smith, W., 1998. New, improved version of the Generic Mapping Tools Released, *Eos Trans., AGU,* **79,** 579.

SUPPORTING INFORMATION

Additional Supporting Information may be found in the online version of this article:

Figure S1. (a) Map (left) and cross-sectional view (right) of the *P*-wave tomography model from Hansen *et al.* (2012), highlighting the superplume structure beneath Africa. (b) Corresponding

images to those shown in (a) but from the current *P*-wave tomography model. Dashed lines in the cross-sections mark the 410 and 660 km discontinuities. On this scale, the two models look very similar and hence interpretations from Hansen *et al.* (2012) also apply to the current model. The main focus of the manuscript, however, is the upper mantle structure beneath Ethiopia/Afar.

Figure S2. Event distribution map. Red circles denote events that are included in the EHB database. Blue circles denote augmented events that were added to the dataset in this study. All augmented events had magnitudes ≥ 5.5 and were located within 30–100° from their corresponding recording station.

Figure S3. (a) Examples of the adaptive grid generated for our current *P*-wave tomography model, shown at selected mantle depths. Darker colors highlight smaller cells, where better sampling of the model is obtained. All cells contain at least 900 hit counts (Hansen *et al.* 2012). Red dashed lines mark the boundaries of the MER. (b) Comparable images to those shown in (a) but for the Hansen *et al.* (2012) tomography model. Comparing these images, one can see that the additional data included in the current model has improved the raypath coverage throughout the study area.

Figure S4. (a) Checkerboard resolution tests, shown at selected mantle depths, from the current *P*-wave tomography model. The input pattern includes 5°-wide anomalies with alternating ±6 per cent velocity variations. All images have been plotted with the same color scale so that the degree of pattern and amplitude recovery can be easily compared. (b) Comparable images to those shown in (a) but for the Hansen *et al.* (2012) tomography model. Comparing these images, one can see that the additional data included in the current model has improved the degree of pattern and amplitude recovery.

Figure S5. Additional resolution tests with synthetic anomalies, comparable to Fig. 3. However, the 'decompression melt anomaly' at shallow mantle depths is now 200-km thick, which is the maximum depth estimated for decompression melting beneath rapidly thinning lithosphere (e.g. Webb & Forsyth 1998) (http://gji.oxfordjournals.org//lookup/supp1/doi:10.1093/gji/ggt116/-/DC1).